J. Biochem. **142,** 731–739 (2007)
doi:10.1093/jb/mvm188

Mutational Analysis of Conserved Outer Sphere Arginine Residues of Chalcone Synthase

Kazuki Fukuma[1], Evan D. Neuls[2], Jennifer M. Ryberg[2], Dae-Yeon Suh[2,*] and Ushio Sankawa[1,3]

[1]Faculty of Pharmaceutical Sciences, Toyama Medical and Pharmaceutical University, Toyama 930-0194, Japan; [2]Department of Chemistry and Biochemistry, University of Regina, Regina, SK S4S 0A2, Canada; and [3]International Traditional Medicine Research Center, Toyama International Health Complex, Toyama 939-8224, Japan

Received August 18, 2007; accepted September 24, 2007; published online October 15, 2007

Chalcone synthase (CHS), a key enzyme in flavonoid biosynthesis, catalyses sequential decarboxylative condensations of *p*-coumaroyl-CoA with three malonyl-CoA molecules and cyclizes the resulting tetraketide intermediate to produce chalcone. Phenylglyoxal, an Arg selective reagent, was found to inactivate the enzyme, although no Arg is found at the active site. Conserved, non-active site Arg residues of CHS were individually mutated and the results were discussed in the context of the 3D structure of CHS. Arg199 and Arg350 were shown to provide important interactions to maintain the structural integrity and foldability of the enzyme. Arg68, Arg172 and Arg328 interact with highly conserved Gln33/Phe215, Glu380 and Asp311/Glu314, respectively, thus helping position the catalytic Cys-His-Asn triad and the ^{372}GFGPG loop in correct topology at the active site. In particular, a mutation of Arg172 resulted in selective impairment in the cyclization activities of CHS and stilbene synthase, a related enzyme that catalyses a different cyclization of the same tetraketide intermediate. These Arg residues and their interactions are well conserved in other enzymes of the CHS superfamily, suggesting that they may serve similar functions in other enzymes. Mutations of Arg68 and Arg328 had been found in mutant plants that showed impaired CHS activity.

Key words: chalcone synthase, outer sphere mutation, stilbene synthase, type III polyketide synthase, site-directed mutagenesis.

Abbreviations: 2-PS, 2-pyrone synthase; BNY, bisnoryangonin; CHS, chalcone synthase; CTAL, *p*-coumaroyltriacetic acid lactone; CTAS, coumaroyltriacetic acid synthase; KAS, β-ketoacyl-acyl carrier protein synthase; PCS, pentaketide chromone synthase; PGO, phenylglyoxal; PKS, polyketide synthase; STS, stilbene synthase; THNS, 1,3,6,8-tetrahydroxynaphthalene synthase.

Chalcone synthase (CHS, E.C. 2.3.1.74) plays a key role in the biosynthesis of plant flavonoids by catalysing consecutive decarboxylative condensations of a phenylpropanoid CoA-ester (*e.g. p*-coumaroyl-CoA) with three C_2 units from malonyl-CoA and subsequent cyclization of the linear tetraketide intermediate to form chalcone, the precursor of diverse flavonoids (Fig. 1). CHS and homologous members of the CHS superfamily, also known as type III polyketide synthases (PKS), are homodimers of 40–45 kDa subunits (*1*, *2*). They are found widely in nature and involved in biosyntheses of diverse natural products that play roles in, among others, UV protection, anti-microbial defense and flower colour in plants, in cyst formation in bacteria and in cell differentiation in amoeba. Stilbene synthase (STS) (*3*), benzalacetone synthase (*4*), benzophenone synthase (*5*), biphenyl synthase (*6*), 2-pyrone synthase (2-PS) (*7*), pentaketide chromone synthase (PCS) (*8*), aloesone synthase (*9*) and coumaroyltriacetic acid synthase (CTAS) (*10*) are representative plant enzymes, while PKS18, a long-chain acylpyrone synthase from *Mycobacterium tuberculosis* (*11*), *1,3,6,8*-tetrahydroxynaphthalene synthase (THNS) from *Streptomyces coelicolor* (*12*), alkylresorcinol synthase from *Azotobacter vinelandii* (*13*) and pentaketide resorcylic acid synthase from *Neurospora crassa* (*14*) have been added to the expanding list of non-plant members of the superfamily (*15*). Further, type III PKS domains of hybrid type I fatty acid-type III PKS enzymes (Steely1 and Steely2) have recently been found in an amoeba, *Dictyostelium discoideum* (*16*). These enzymes differ from CHS in their choice of starter-CoA units, the number of condensation reactions catalysed and the cyclization mechanism by which the intermediate oligoketide is cyclized. Enzymes of the CHS superfamily invariably contain catalytic residues of Cys164, His303 and Asn336 [sequence numbering based on *Pueraria lobata* CHS and *Medicago sativa* CHS (MsCHS)]. However, subtle differences in enzyme active sites lead to the observed enzyme diversity. STS, which shares >65% amino acid sequence identity with CHS, also catalyses the condensation reactions of three molecules of malonyl-CoA with *p*-coumaroyl-CoA, but the resulting tetraketide intermediate is cyclized

*To whom correspondence should be addressed. Tel: +1-306-585-4239, Fax: +1-306-337-2409, E-mail: suhdaey@uregina.ca

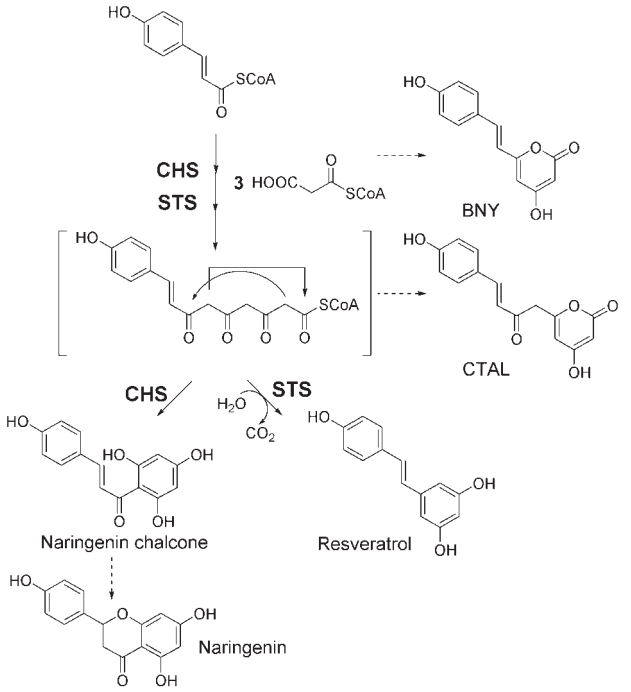

Fig. 1. **Reactions catalysed by CHS and STS.** Both CHS and STS first catalyse the decarboxylative condensations of three acetate residues from malonyl-CoA with *p*-coumaroyl-CoA starter unit to form a common tetraketide intermediate. Then, CHS subsequently cyclizes the intermediate *via* Claisen-type acylation involving C-1 and C-6 to give naringenin chalcone, while STS cyclizes the same intermediate to give resveratrol *via* aldol-type cyclization that includes hydrolysis and decarboxylation. Naringenin chalcone produced by CHS is *non-enzymatically* converted to naringenin under reaction conditions used. BNY and CTAL, the derailment by-products after two and three steps of condensations, respectively, are also produced in both enzyme reactions *in vitro*.

via decarboxylative aldol-type reaction to give stilbene (Fig. 1). In the STS-catalysed stilbene formation, a hydrogen bond activated water molecule found at the active site cavity (dubbed as 'aldol switch') was proposed to participate in the hydrolysis of the tetraketide intermediate thioester prior to cyclization (*3*, *17*).

Numerous studies have established that mutations on non-active site residues often affect enzyme activity, and insights into enzyme mechanism can be gained by studying such outer sphere mutations (*18*, *19*). Earlier studies on the effects of chemical modification with amino acid selective reagents on CHS activity showed that thiol-selective and imidazole-selective reagents (iodoacetamide and diethyl pyrocarbonate, respectively) inactivate CHS, in agreement with the importance of catalytic Cys and His residues in CHS (*20*, *21*). Interestingly, phenylglyoxal (PGO), an Arg-selective reagent, also completely abolished enzyme activity, although no Arg residue other than Arg58, which is located at the entrance of the substrate binding tunnel, is found at the active site of CHS. Further, a 'leaky' mutation leading to a temperature-sensitive phenotype in *Arabidopsis* was shown to be due to an Arg to Cys mutation in CHS (*22*). Arg residues, largely protonated at physiological pH, are well suited to play structural roles by forming salt bridges with anionic amino acids. These observations led us to investigate mutational effects of highly conserved Arg residues of CHS (Arg 58, Arg68, Arg172, Arg 199, Arg328 and Arg350) to reveal intricate non-covalent interactions that play critical structural roles in positioning the catalytic active site residues in CHS and, likely, in other homologous enzymes.

MATERIALS AND METHODS

Site-directed Mutagenesis—Mutants of *P. lobata* CHS (Databank accession no. P23569**)** were constructed by the PCR megaprimer method (*23*), which employs two flanking primers, one mutagenic primer and two rounds of PCR. The pET-32a(+) vector (Novagen) containing the CHS gene (pET-CHS) (*24*) was used as template in the PCR. The forward flanking primer was 5′-GACAAGGCCA*TG*GTGAGCGTA-3′ (the start codon is in italic and the *Nco*I site underlined) and the reverse flanking primer was 5′-TGTGGATCCAAACTCCAGCAA GT-3′ (the *Bam*HI site underlined). Following the first PCR with the mutagenic primer (Table S1, Supplementary data) and an appropriate flanking primer (5 min at 94°C, 20 cycles of 1 min at 94°C, 1 min at 50–55°C, 2 min at 72°C and 5 min of final extension at 72°C), the second PCR (5 min at 94°C, 35 cycles of 1 min at 94°C, 1 min at 50–60°C, 2 min at 72°C and 5 min of final extension at 72°C) was carried out with another flanking primer and the first PCR products (megaprimer), giving one 1.2 kb full-length DNA fragment containing the desired mutation. The *Nco*I–*Bam*HI digested mutant CHS fragment was ligated into the *Nco*I–*BamH*I digested pET-32a(+) vector and the ligation mixture was transformed into *Escherichia coli* NovaBlue competent cells (Novagen). For mutagenesis using the Quick Change protocol (Stratagene), the pET-CHS or the pET-STS plasmid harbouring *Arachis hypogaea* STS **(**AB027606**)** (*24*) and a pair of complementary mutagenic primers containing desired mutation (Table S1, Supplementary data) were used in PCR reactions to create the mutated plasmid. When possible, a restriction site was introduced or removed in mutagenic primers for easy screening of mutated plasmid. The mutagenesis was further confirmed by sequencing of the PCR products.

Protein Expression and Purification—Wild-type and mutant CHS and STS were expressed as thioredoxin–HisTag-fusion proteins for improved solubility and facile purification. Expression, induction and purification with Ni^{2+}-chelation chromatography were carried out as previously described (*24*).

Enzyme Assay and Steady-state Kinetic Analysis—The standard assay mixture (0.1 ml) for determination of condensing activity of the enzymes contained appropriate amounts of enzyme, 100 μM *p*-coumaroyl-CoA and 20 μM [2-^{14}C]malonyl-CoA (2.2 GBq/mmol, NEN) in 100 mM potassium phosphate buffer, pH 7.2, containing 10% glycerol, 0.1% Triton X-100, and 1 mM dithiothreitol. After incubation at 37°C for 20–30 min, the reaction was terminated by acidification (7.5 μl of 1 N HCl) to a final pH of 4 and the reaction products were extracted with 200 μl of ethyl acetate. A portion (50 μl) of the extract was analysed by TLC on RP18 plates (Art. 1.15389, Merck)

with methanol : H_2O : acetic acid (60 : 40 : 1, v/v/v) as solvent. The radioactive products were quantified with an imaging plate analyser (BAS2000, Fuji or Molecular Dynamics Storm 860, Amersham Pharmacia) using standards of known specific activity. Authentic naringenin (R_f = 0.3) and resveratrol (R_f = 0.5) were used as internal standards to identify the products. Derailment products, bisnoryangonin (BNY) and *p*-coumaroyltriacetic acid lactone (CTAL), were identified from their R_f values (BNY, R_f = 0.4; CTAL, R_f = 0.6) (*25*).

Malonyl-CoA decarboxylase activity was determined by following acetyl-CoA formation (*26*). At the end of the enzyme reaction (20 min at 37°C) in 0.1 M HEPES, pH 7.0, with 100 μM [2-^{14}C]malonyl-CoA, a portion (10–20 μl) of aqueous phase was analysed on silica 60 TLC plates (Art. 1.11798, Merck) with isopropanol : H_2O : 25% ammonia water (80 : 5 : 15, v/v/v) as solvent to separate acetyl-CoA (R_f = 0.6) from remaining malonyl-CoA (R_f = 0.25). The specific enzyme activity was expressed in picomoles of the product produced per second per milligram (pkat/mg).

Kinetic experiments were performed in 0.1 M HEPES, pH 7.0, as described previously (*24*). The $K_{m(app)}$-values for *p*-coumaroyl-CoA in the condensing reaction were determined at a malonyl-CoA concentration of 10 μM, while those for malonyl-CoA were determined at 100 μM *p*-coumaroyl-CoA. The $K_{m(app)}$-values for malonyl-CoA in malonyl-CoA decarboxylation were determined in the absence of *p*-coumaroyl-CoA. For each experiment, five substrate concentrations covering the range of 0.2–5 $K_{m(app)}$ were employed. Obtained *v* against [S] data were fit to the Michaelis–Menten equation using a non-linear regression program (Enzyme Kinetics Pro, ChemSW) to calculate V_{max} and $K_{m(app)}$ values.

Other Methods—CHS or STS (16 μM) was pre-incubated with 2 mM PGO (*27*) in 85 mM $NaHCO_3$ buffer, pH 8.3, for 30 min at 25°C in the dark. The reaction was quenched with 2 mM Arg and 10 μl of 100 μl total reaction mixture were drawn for the enzyme activity measurement under standard conditions as described earlier. *p*-Coumaroyl-CoA was prepared chemically from the respective *N*-hydroxysuccinimide ester according to Stöckigt and Zenk (*28*), or enzymatically from coumaric acid and CoASH using tobacco 4-coumarate: coenzyme A ligase (4-CL) as described by Beuerle and Pichersky (*29*). Protein concentration was determined by the Bradford dye assay (Bio-Rad) with bovine serum albumin as standard. Amino acid sequence alignments were created using ClustalX (*30*) with BLOSUM series alignment matrix. Homology modelling of the 3D structure of *P. lobata* CHS, of which amino acid sequence shows 91% identity and contains only four non-conservative substitutions as compared to the MsCHS sequence, was carried out with the SWISS-MODEL package (*31*), using the structure of MsCHS (PDB i.d. 1bi5) as structural template. The protein structures were analysed with DeepView program (v.3.7) (*32*).

RESULTS AND DISCUSSION

Chemical Modification, Mutagenesis and Mutant Analysis—Treatment with 2 mM PGO almost completely abolished the enzyme activity of CHS and STS. However, the two enzymes reacted with PGO in a different fashion. While the presence of malonyl-CoA (0.5 mM) during modification failed to provide protection for both enzymes, *p*-coumaroyl-CoA (0.3 mM) provided a partial protection only for STS. These data indicated that non-active site Arg residue(s) in CHS and STS play critical role(s) in CHS- and STS-catalysed reactions. Sequence alignments of over 100 selected plant CHS superfamily sequences containing all non-CHS enzymes and representative CHSs from different taxa revealed six highly conserved Arg residues, R58, R68, R172, R199, R328 and R350 (Supplementary data). In this study, these Arg residues are individually mutated either to Leu or to Gln, which have comparable conformational preferences with Arg (*33*), to minimize conformational perturbation. In addition, Arg to Gln is one of frequently accepted point mutations (*34*).

An expression protocol involving induction at 25°C for 20 h was used throughout the study. Mutants were purified under identical conditions to those used for the wild-type enzymes. Purified mutants were analysed for their ability to catalyse malonyl-CoA decarboxylation, condensing (chain elongation) and cyclization reactions. Since earlier studies showed no functional difference between thioredoxin-fusion and native enzymes recovered after removing the fusion part by enterokinase cleavage (*10*, *24*), more stable thioredoxin-fusion proteins were used for further study. The assay and analysis conditions used in this study permitted simultaneous analysis of derailment products, BNY and CTAL as well as the cyclized end-products, enabling us to assess the effects of mutation on different steps of the catalytic cycle (Fig. 1) (*10*, *24*, *25*).

Arg58, Arg199 and Arg350—Among 105 sequences examined, Arg58 is conserved in all but eight sequences. Exceptions of non-conservative substitutions are *Ruta graveolens* acridone synthases (S60241 and Q9FSC0) containing Thr residues, and *Rheum palmatum* aloesone synthase (AAS87170) containing Phe at the corresponding position. No non-conservative substitution was found for Arg199, while some anther-specific CHS homologs (*35*) have hydrophobic residues at the position of Arg350 (Leu in an *Arabidopsis thaliana* homolog, CAB45446; Ile in a *Silene latifolia* homolog, BAE80096; Val in an *Aegilops tauschii* homolog, CAJ13966).

Yield (foldability) and products profile of CHS-R58L were similar to those of wild-type CHS (Figs. 2, 3, Table 1). However, $K_{m(app)}$ values for malonyl-CoA of the mutant increased 4-fold, when measured for chalcone production and for malonyl-CoA decarboxylation (Table 2). The mutant showed 2-fold (condensing) to 9-fold (malonyl-CoA decarboxylation) decrease in specific activity determined under standard conditions (Table 1), which was due to increased $K_{m(app)}$ values for malonyl-CoA, as V_{max} values remained relatively unaffected by the mutation (Table 2). Interestingly, $K_{m(app)}$ for *p*-coumaroyl-CoA in the condensing reaction was comparable to that of wild-type, reflecting the complexity of the multi-step reactions catalysed by CHS and kinetic insignificance of the initial binding of *p*-coumaroyl-CoA in the overall catalysis. The observed biochemical characteristics of CHS-R58L are consistent with the fact that Arg58 is located at the entrance of CoA binding site and serves as a part of CoA docking points

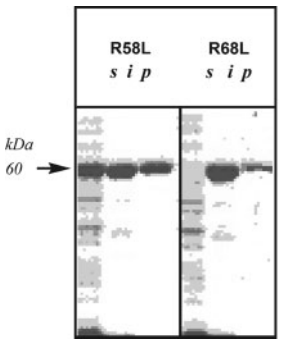

Fig. 2. **SDS-PAGE of CHS-R58L and CHS-R68L mutants.** Solubility and purity of mutant were visualized with SDS-polyacrylamide gel electrophoresis. *s*, Soluble fraction; *i*, insoluble fraction; *p*, purified protein after Ni^{2+}-affinity chromatography. Mutants were expressed in *E. coli* as thioredoxin-fusion proteins (60 kDa, arrow). Yields of other mutants were in-between these two mutants (Table 1). Proteins were separated on a 12% (w/v) acrylamide minislab gel and stained with Coomassie Brilliant Blue R250.

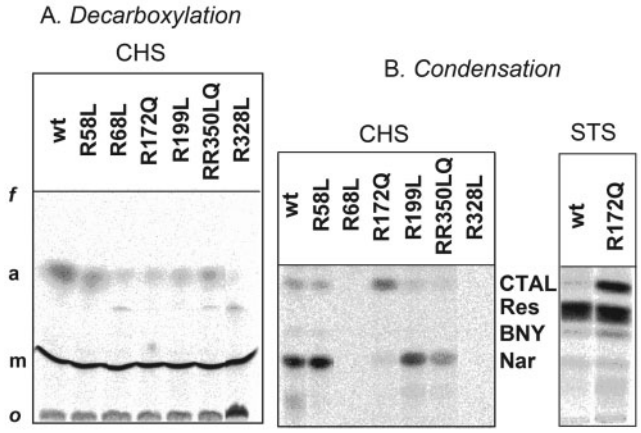

Fig. 3. **Radio-TLC analysis of the reaction products produced by the wild-type and Arg mutants of CHS and STS.** (A) Malonyl-CoA decarboxylation activity: the enzyme reaction was carried out in the presence of 100 μM [2-^{14}C]malonyl-CoA in 0.1 M HEPES buffer, pH 7.0. Acetyl-CoA (a, R_f = 0.6) and malonyl-CoA (m, R_f = 0.25) were separated on silica 60 plate. (B) Condensing activity: the enzyme reaction was carried out with 100 μM *p*-coumaroyl-CoA and 20 μM [2-^{14}C]malonyl-CoA. Ethyl acetate extracts of the reaction mixture were analysed on RP18 plate. The reaction products as well as derailment products are indicated.

(*36*) (Fig. 4A). In the 3D structure of MsCHS complexed with malonyl-CoA (PDB i.d., 1cml), one of the guanidinium nitrogens of Arg58 is in hydrogen-bonding distances (2.48 Å and 3.98 Å) from the two oxygens of 3′-ribose phosphate of CoA. In this role, Arg58 in CHS is equivalent to Arg36 in *E. coli* β-ketoacyl-acyl carrier protein synthase (KAS) II (*37*), whereas *E. coli* KAS III has no counterpart (*38*).

Arg199 and Arg350 are located 14 and 22 Å away from the active site Cys, respectively (Fig. 4A). The side chain of Arg199 forms hydrogen bonds with the backbone carbonyl oxygens of the neighbouring Val261 (Ala261 in MsCHS) and Leu263 residues, while the two N(η) atoms of Arg350 are close (2.9 Å) to the carboxylic oxygen atoms of highly conserved Glu116, thus bringing together the N-end and C-end parts of the enzyme. Mutations of these two Arg residues resulted in decreased yields (Table 1). R199L and R350L/R351Q were similar to wild-type in products profile and showed modestly decreased activity. Numerous studies have revealed residues that are specifically important for protein folding (*39*). Both Arg199 and Arg350 of CHS fall into this type of residues, since mutations on these residues greatly influence the foldability of the protein without drastic effects on enzyme activity.

Arg68—Arg68 is absolutely conserved among the sequences examined except *Psilotum nudum* STS (BAA87925), which has KK^{78}*V*H in place of KK^{68}*R*Y in CHS. The yield of purified CHS-R68L was <1% of that of wild-type (Fig. 2, Table 1). Condensing activity of CHS-R68L was not detected, even when assayed with 20 μg of protein (Fig. 3B). However, with 10 μg of protein, a weak malonyl-CoA decarboxylase activity was observed, though the specific activity was about 8% of that of wild-type (Table 1, Fig. 3A). The mutant exhibited a modest increase (1.6-fold) in $K_{m(app)}$ for malonyl-CoA, but more than 10-fold decrease in V_{max} (Table 2). In the homology modelled structure of *P. lobata* CHS as well as in the crystal structure of MsCHS, one of the two N(η) atoms of R68 is within hydrogen-bonding distance of the side chain amide oxygen of Gln33 (2.9–3.0 Å) (Table 3). The other N(η) atom is within the hydrogen-bonding distance of the backbone carbonyl oxygen of Phe215 (2.9 Å) (Fig. 4B). Also, the two N atoms are <3 Å away from the backbone carbonyl oxygens of Gln212 and Ala213. Both Gln33 and Phe215 are highly conserved in the CHS superfamily, and these hydrogen bonds of Arg68 to Glu33 (Thr21 in THNS) and Phe215 are also observed in all the enzymes of the CHS superfamily of known crystal structures, MsCHS (*36*), *Pinus sylvestris* STS (*3*), *A. hypogaea* STS (*17*), *Gerbera hybrida* 2-PS (*7*), *Aloe arborescens* PCS (*8*), *S. coelicolor* THNS (*12*), *M. tuberculosis* PKS18 (*11*), and *D. discoideum* Steely1 (*16*) (Table 3). Taken together, these data suggested that R68 play dual roles in CHS. First, it plays a role in maintaining correct conformation (foldability) by bringing the enzyme's N-end part (Gln33) together with the core active site (Phe215) of the enzyme via hydrogen bonds. Arg68 also fixes Phe215 in the correct position in the active site. Phe215, located at the junction between the active site cavity and the CoA binding tunnel of CHS, has been proposed to facilitate decarboxylation of malonyl-CoA by providing a non-polar environment, and to help orient substrates and intermediates during the sequential condensation reactions (*4*, *36*, *40*). Our results provide another support for the involvement of Phe215 in the CHS catalysis, as Phe215 mutants thus far prepared generally showed marked decrease in malonyl-CoA decarboxylase activity and produced more truncated, derailment products (*4*, *40*, *41*).

During the course of this study, a white-flowering phenotype of *Matthiola incana* (hoary stock) was shown to be due to a single nucleotide substitution that led to a mutation of the same Arg (Arg72 in *M. incana* CHS) to

Table 1. **Expression, product profile, and enzyme activity of the Arg mutants of CHS and STS.**

	Yield[a] mg/100 ml culture	Product profile[b] (mol%)				Specific activity (pkat/mg)	
		Naringenin	CTAL	BNY	Resveratrol	C_2-unit condensation[b]	Malonyl-CoA decarboxylation[c]
CHS							
Wild-type	5.3 ± 0.96	76 ± 4.0	18 ± 0.36	2.9 ± 2.5	3.5 ± 1.2	110 ± 38	250 ± 27
R58L	5.6 ± 0.55	88 ± 0.91	10 ± 0.96	1.2 ± 0.40	1.0 ± 0.96	54 ± 1.9	27 ± 2.1
R68L	0.039 ± 0.007					Inactive	21 ± 2.9
R172Q	3.0 ± 0.25	18 ± 0.91	70 ± 0.62	11 ± 0.71	0.59 ± 0.031	6.7 ± 0.087	4.4 ± 0.28
R199L	1.4 ± 0.36	60 ± 4.2	24 ± 3.1	5.5 ± 2.4	1.1 ± 1.4	40 ± 5.2	91 ± 11
R328H	1.9 ± 0.42	72 ± 9.9	20 ± 4.2	5.2 ± 2.4	2.7 ± 1.0	68 ± 20	7.7 ± 0.79
R328L	0.79 ± 0.30					Inactive	Inactive
R350L/R351Q[d]	0.065 ± 0.014	80 ± 0.50	14 ± 0.21	3.8 ± 0.17	2.6 ± 0.49	37 ± 4.6	74 ± 4.8
STS							
Wild-type	5.0 ± 1.2	2.1 ± 0.91	2.3 ± 1.2	3.8 ± 0.7	92 ± 2.8	140 ± 17	87 ± 5.9
R172Q	3.1 ± 0.9	2.0 ± 0.45	37 ± 2.2	5.0 ± 1.3	56 ± 3.6	110 ± 10	74 ± 5.6

[a]Yields are calculated after purification by Ni^{2+}-chelation chromatography.
[b]The reaction was performed in 0.1 M potassium phosphate, pH 7.2, containing 10% glycerol, 0.1% Triton X-100 and 1 mM dithiothreitol with 0.1 mM *p*-coumaroyl-CoA and 20 μM [2-^{14}C]malonyl-CoA as substrates. Specific activity is defined as picomoles of condensed C_2-units per second per milligram protein (pkat/mg).
[c]The reaction was performed in 0.1 M HEPES, pH 7.0, with 100 μM [2-^{14}C]malonyl-CoA as sole substrate. The amounts of the enzymes added in the reaction were the wild-type, R328H and RR350LQ mutants, 2 μg; R58L, R119L and R172Q mutants, 5 μg; R68L and R328L mutants, 10 μg. Specific activity is defined as picomoles of acetyl-CoA produced per second per milligram protein (pkat/mg).
[d]In addition to R350L mutation, Arg351, which is not conserved, was also mutated to Gln to introduce a restriction site for facile mutant screening.
Data are indicated as means ± SD (n = 3).

Table 2. **Kinetic parameters of the wild-type and Arg mutants of CHS.**

	Condensing reaction[a]			Malonyl-CoA decarboxylation	
	$K_{m(app)}$		V_{max} pmol/s/ml	$K_{m(app)}$ μM	V_{max} pmol/s/ml
	p-Coumaroyl-CoA μM	Malonyl-CoA μM			
Wild-type	50 ± 7.1	2.2 ± 0.78	0.44 ± 0.084	28 ± 7.5	8.3 ± 0.34
R58L	43 ± 4.1	9.3 ± 0.84	0.45 ± 0.21	110 ± 19	5.2 ± 0.30
R68L				44 ± 9.5	0.81 ± 0.25
R172Q	53 ± 1.9	2.5 ± 0.52	0.036 ± 0.012	32 ± 5.2	1.3 ± 0.35
R328H	40 ± 8.3	1.9 ± 0.75	0.48 ± 0.14	10 ± 4.0	1.7 ± 0.96

[a]$K_{m(app)}$ and V_{max} values were calculated for naringenin production except for the R172Q mutant, where the values were for CTAL production.
Data are expressed as means ± SD (n = 3).

Ser in the *chs* gene (*42*). Unlike the R68L mutant of this study, the recombinant *M. incana* R72S mutant was expressed in soluble form, likely due to the less disruptive effect of the Arg to Ser mutation on protein folding. Nonetheless, the *M. incana* R72S mutant also totally lacked chalcone formation activity, although its malonyl-CoA decarboxylase activity was not measured. The mutational effects of R72S were also explained in terms of the loss of the hydrogen bonds between the Arg and the Gln and Phe residues (*42*).

Arg172—Arg172 is absolutely conserved in the CHS superfamily examined. CHS-R172Q showed a relatively high yield (>50% of wild-type); however, its specific activity decreased 16-fold in condensing reaction and 57-fold in malonyl-CoA decarboxylation. Comparable $K_{m(app)}$ values but significantly decreased V_{max} values indicated that enzyme turnover was impaired. A more significant finding was a sharp increase in CTAL (the derailment product at the stage of tetraketide) formation by the mutant (Fig. 3B). While the production ratio of CTAL to naringenin under the standard assay conditions was close to 0.3 in wild-type CHS, it was 3.9 in the R172Q mutant, indicating that the ability to catalyse cyclization was severely damaged in this mutant. The same mutation of R172Q had similar effects on the STS-catalysed cyclization. Hence, STS-R172Q also produced more CTAL at the expense of resveratrol, although the effect was not as dramatic as in CHS (Table 1, Fig. 3B). The N(ε) atom and one of two N(η) atoms in the guanidinium group of Arg172 form hydrogen/ionic bonds to the two side chain oxygens of highly conserved Glu380 (Fig. 4C). Arg172 is located in the middle of the α-helix that follows the catalytic nucleophile, Cys164, and Glu380 is in the β-sheet immediately following the ^{372}GFGPG loop. Therefore, the Arg172 ··· Glu380 interactions seem to be instrumental in maintaining correct

configuration of the loop relative to the active site Cys164, to which growing intermediates are attached during catalysis. The ^{372}GFGPG loop makes up a part of active site sidewall (*36*). Similar loops are found in other condensing enzymes such as thiolases, KAS I, II and III and 3-hydroxy-3-methylglutaryl-CoA (HMG-CoA) synthases (*43*). However, all the enzymes of the CHS superfamily contain a Pro in the loop, while other condensing enzymes contain either Gly or Ser (for example, ^{303}AFG*G*G in *E. coli* KAS III). Earlier, the Pro375 to Gly mutation in CHS and STS was shown to cause substantial increase in the production ratio of CTAL to cyclized product (0.3–0.9 in CHS and 0.1–1.6 in STS) (*24*). Hence, it was proposed that the ^{372}GFGPG loop is important for correct folding of the tetraketide intermediate prior to ring formation in CHS- and STS-catalysed reactions (*24*). The results obtained in this study agree well with the role of the loop in serving as a part of the active site scaffold on which the stereochemistry of cyclization is carried out. The R172Q mutants of CHS and STS may become useful research tools in studying the two different cyclization reactions catalysed by CHS and STS in detail.

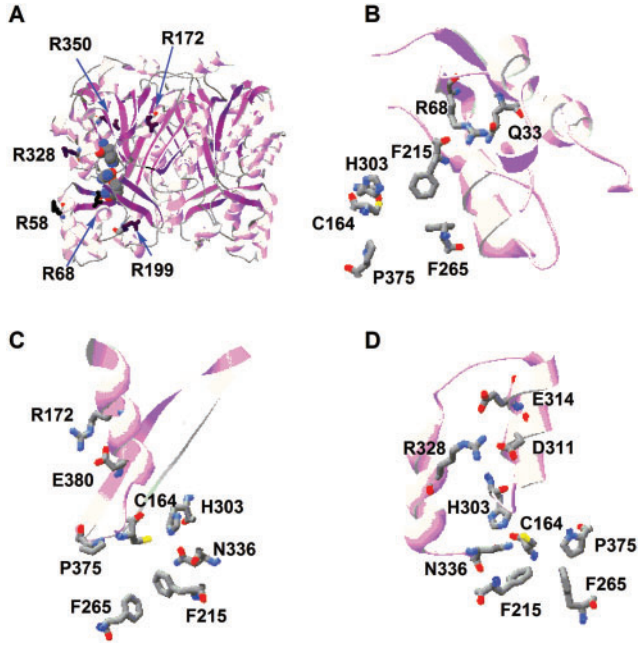

Fig. 4. **Homology-modelled overall structure of *P. lobata* CHS and local structures surrounding the conserved Arg residues.** (A) Ribbon diagram of the CHS homodimer. Catalytic His303 and Asn336 are shown in space-filling model to indicate the active site. The locations of the six Arg residues are also shown. Except Arg58, the other five Arg residues are buried inside of the protein. Arg68 and Gln33 (B), Arg172 and E380 (C) and Arg328 and Asp311/Glu314 (D) are shown as well as the active site residues (Cys164, F215, F265, His303, Asn336 and Pro375). For another view on R68, see Fig. 5 in Ref. (*42*).

Hydrangea macrophylla CTAS, which shares 74% amino acid identity with CHS from the same plant, is devoid of the ability to catalyse cyclization and produces CTAL as the main product *in vitro* using *p*-coumaroyl-CoA as starter substrate (*10*). However, as the corresponding Arg and Glu residues are also conserved in CTAS (Arg176 and Glu390), a different strategy is likely responsible for the inability of CTAS to catalyse cyclization. The Arg172···Glu380 interactions are also observed in the crystal structures of other plant enzymes (Table 3). Among the three non-plant enzymes whose structures have been determined, similar interactions are observed in THNS and Steely1, while, in *M. tuberculosis* PKS18, Asn is found at the corresponding position of Arg172. PKS18 produces pyrones as main products *in vitro*, however it may not catalyse cyclization reaction (lactonization) *in vivo* (*11*).

Arg328—Among the sequences examined, Arg328 is conserved in all but three enzymes; the two *R. graveolens* acridone synthases have Lys and *Plumbago indica* hexaketide synthase (BAF44539) has Trp instead. The two N(η) atoms of the Arg328 guanidinium group are in close distances (2.5–3.6 Å) from the side chain carboxylic

Table 3. **Interactions of the conserved Arg residues with other residues observed in the crystal structures of the enzymes of the CHS superfamily.**

Enzyme	PDB i.d.	Conserved Arg residue		
		R68	R172	R328
MsCHS	1bi5	Q33 (2.90) R68 (2.87) F215(C=O)	R172 (Nε, 2.75; Nη, 2.92) E380	D311 (2.63, 3.01) R328 (3.38) E314
PlCHS[a]		Q33 (2.96) R68 (2.89) F215(C=O)	R172 (Nε, 2.85; Nη, 2.99) E380	D311 (2.74) R328 (3.34) E314
PsSTS	1u0u	Q35 (2.99) R70 (2.75) F215(C=O)	R175 (Nε, 2.88; Nη, 2.54) E383	D314 (2.46, 3.20) R331 (3.60) E317
AhSTS	1z1e	Q33 (3.16) R68 (3.07) F215(C=O)	R172 (Nε, 3.10; Nη, 2.92) E380	D311 (2.74, 3.19) R328 (2.97) E314
2-PS	1ee0	Q38 (3.11) R73 (2.98) F220(C=O)	R177 (Nε, 2.90; Nη, 3.00) E385	D316 (3.02) R333 (3.16) E319
AaPCS	2d3m	Q43 (2.78) R78 (2.80) F225(C=O)	R172 (Nε, 2.85; Nη, 2.99) E380	D311 (2.74) R333 (3.34) E314
THNS	1u0m	T21 (3.04) R50 (2.96) F188(C=O)	R147 (3.48) E340	D278 (3.70) R295
PKS18	1ted	Q49 (3.21) R81 (2.78) F224 (C=O)	*N180 (3.17; 3.75) E384*	*I320 (3.5∼4.2) W338*
Steely1	2h84	Q2803 (2.86) R2836 (2.56) F2979(C=O)	R2938(Nε, 2.91; Nη, 2.85) E3139	*L3078 (3.9∼4.1) W3096*

[a]Homology model was constructed with the SWISS-MODEL package, using the structure of MsCHS (PDB i.d. 1bi5) as structural template. Distances in Å are given in parentheses. Amino acids that interact with the conserved Arg residue and the distances between the side chain atoms are given schematically. For instance, 'Q33 (2.90) R68 (2.87) F215(C=O)' illustrates that the distances from the side chain nitrogen atoms of Arg68 to the side chain oxygen of Gln33 and to the backbone carbonyl oxygen of Phe215 are 2.90 Å and 2.87 Å, respectively. Non-conservative interactions are in italic. MsCHS, *Medicago sativa* CHS; PlCHS, *Pueraria lobata* CHS; PsSTS, *Pinus sylvestris* STS; AhSTS, *Arachis hypogaea* STS; 2-PS, *Gerbera hybrida* 2-PS; AaPCS, *Aloe arborescens* PCS; THNS, *Streptomyces coelicolor* THNS; PKS18, *Mycobacterium tuberculosis* PKS18; Steely1, *Dictyostelium discoideum*.

oxygens of Asp311 and Glu314, both of which are also highly conserved in the CHS superfamily (Fig. 4D, Table 3). Arg328 is located in the middle of the α-helix preceding Asn336, and Asp311 and Glu314 are in the α-helix following His303. Both His303 and Asn336 are catalytic residues of CHS and play critical roles in malonyl-CoA decarboxylation and condensation reactions (*36*, *40*). Thus, Arg328 along with Asp311 and Glu314 serve to bring these two catalytic residues together in correct positions at the active site.

CHS-R328K was similar to the wild-type in yield, products profile and activity. However, CHS-R328L exhibited a low yield (15% of wild-type) (Table 1) and virtually no activity, even when assayed with 20 μg of protein (Fig. 3), indicating the importance of the positive charge in Arg328 for enzyme function. Similar mutational effects of Arg328 were observed in STS; STS-R328K was similar to wild-type STS in enzymatic properties, but virtually all STS-R328L mutant protein was recovered in insoluble fractions (data not shown). The structural effect of the Arg to Leu mutation in CHS was further probed by measuring reactivity toward a chemical modification reagent. CHS contains a single cystein residue that reacts readily to 5,5'-dithio-bis (2-nitrobenzoic acid) (DTNB) at neutral pH. The reactive cystein residue was not Cys164 as might have been expected, since CHS-C164S showed similar behaviour towards DTNB labelling (data not shown). When reactivity toward DTNB of CHS-R328L was compared to that of wild-type under identical conditions, the R328L mutant showed an 8-fold increase in second-order rate constant ($80\,M^{-1}s^{-1}$ versus $10\,M^{-1}s^{-1}$ in wild-type) for 2-nitro-5-mercaptobenzoic acid production, suggesting that the reactive Cys is more exposed in CHS-R328L, probably due to local perturbation in protein conformation.

When Arg328 was mutated to His in CHS, the resulting CHS-R328H exhibited moderate yield (36% of wild-type) and reactivity toward DTNB (4-fold increase from that of wild-type), indicating that the conformational perturbation observed in the R328L mutant was somewhat compensated for in CHS-R328H. In line with this, CHS-R328H showed comparable products profile and condensing activity to those of wild-type. One notable distinction was a marked decrease (30-fold) observed in malonyl-CoA decarboxylase activity of the mutant (Table 1). His303 was shown to function as a base to activate the nucleophile Cys (*20*, *21*). Also, His303 and Asn336 were proposed to function as an oxyanion hole for stabilization of the charge on the oxo group of malonyl unit during malonyl-CoA decarboxylation (*40*). Mutation of Arg328 to His may have caused a local perturbation of relative positioning of these two catalytic residues and led to the observed decrease in activity of CHS-R328H. In CHS-R328H, decarboxylation activity was more severely affected than condensing activity. CHS catalyses multiple reactions, and it is difficult to decipher mutational effect on individual catalytic steps. As each condensing event involves decarboxylation of malonyl-CoA, the observation that decarboxylation activity was more severely affected than condensing activity in CHS-R328H suggested that the C–C bond formation is slow and rate-limiting, at least in the CHS-R328H-catalysed decarboxylative condensation, and that the conformational disturbance caused by the mutation have more detrimental effect during decarboxylation.

The interactions of Arg328 with the two acidic residues, Asp311 and Glu314, are also found in the crystal structures of other plant enzymes (Table 3). In PKS18 and Steely1, these charged residues are substituted with bulky hydrophobic residues. Trp338 in PKS18 and Trp3096 in Steely1 are in close distances (~4 Å) from Ile320 and Leu3078, respectively, indicating that the electronic interactions involving Arg328 in CHS and other enzymes are replaced with van der Waals interactions in PKS18 and Steely1 (Table 3). Recently, a 'leaky' temperature-sensitive phenotype of *Arabidopsis*, *tt4*(UV25), was found to be caused by a single mutation of Arg328 (Arg334 in the *Arabidopsis* enzyme) to Cys (*44*). The mutant plant accumulated reduced levels of CHS enzyme and flavonoids possibly in a temperature-sensitive manner. Based on the results from northern blot and *in planta* protein cross-linking experiments, the observed lower level of the *Arabidopsis* CHS-R334C mutant was attributed to the effects of the mutation on protein stability and possibly on reduced ability of the mutant CHS to form functional homodimer, although Arg328 (Arg334) is located on the opposite side of the protein from the dimerization interface (*22*).

In conclusion, mutational analysis of six highly conserved, non-active site Arg residues in CHS was performed. Arg199 and Arg350 were shown to provide important interactions to maintain the structural integrity and foldability of the enzyme. Mutations on Arg68, Arg172 and Arg328 greatly affected enzyme activity, and the mutational effects were traced to the fact that these residues play 'docking' roles in positioning active site residues in correct catalytic topology. These results illustrate that residues remote from the active site can have substantial effects on the catalytic activity of an enzyme. The Arg residues studied here are conserved in the enzymes of the CHS superfamily, suggesting that these conserved Arg residues may serve similar functions in other enzymes of the CHS superfamily. Mutations of the two Arg residues, Arg68 and Arg328, had been found in mutant plants.

Supplementary data are available at *JB* online.

Financial supports were provided from the Ministry of Education, Science, Sports and Culture of Japan (to U.S.), the Tokyo Biochemistry Research Foundation, Japan (to D.-Y.S), and the Natural Sciences and Engineering Research Council of Canada (NSERC) (to D.-Y.S.). The authors thank Drs T. Buerle and E. Pichersky for their kind gift of the plasmid harbouring tobacco 4-CL. E.D.N. and J.M.R. were recipients of NSERC Undergraduate Student Research Awards.

REFERENCES

1. Schröder, J. (1997) A family of plant-specific polyketide synthases. Facts and predictions. *Trends Plant Sci.* **2**, 373–378
2. Austin, M.B. and Noel, J.P. (2003) The chalcone synthase superfamily of type III polyketide synthases. *Nat. Prod. Rep.* **20**, 79–110

3. Austin, M.B., Bowman, M.E., Ferrer, J.L., Schröder, J., and Noel, J.P. (2004) An aldol switch discovered in stilbene synthases mediates cyclization specificity of type III polyketide synthases. *Chem. Biol.* **11**, 1179–1194
4. Abe, I., Sano, Y., Takahashi, Y., and Noguchi, H. (2003) Site-directed mutagenesis of benzalacetone synthase. *J. Biol. Chem.* **278**, 25218–25226
5. Liu, B., Falkenstein-Paul, H., Schmidt, W., and Beerhues, L. (2003) Benzophenone synthase and chalcone synthase from *Hypericum androsaemum* cell cultures: cDNA cloning, functional expression, and site-directed mutagenesis of two polyketide synthases. *Plant J.* **34**, 847–855
6. Liu, B., Raeth, T., Beuerle, T., and Beerhues, L. (2007) Biphenyl synthase, a novel type III polyketide synthase. *Planta* **225**, 1495–1503
7. Jez, J.M., Austin, M.B., Ferrer, J., Bowman, M.E., Schröder, J., and Noel, J.P. (2000) Structural control of polyketide formation in plant-specific polyketide synthases. *Chem. Biol.* **7**, 919–930
8. Morita, H., Kondo, S., Oguro, S., Noguchi, H., Sugio, S., Abe, I., and Kohno, T. (2007) Structural insight into chain-length control and product specificity of pentaketide ch2romone synthase from *Aloe arborescens*. *Chem. Biol.* **14**, 359–369
9. Abe, I., Watanabe, T., Lou, W., and Noguchi, H. (2006) Active site residues governing substrate selectivity and polyketide chain length in aloesone synthase. *FEBS J.* **273**, 208–218
10. Akiyama, T., Shibuya, M., Liu, H.M., and Ebizuka, Y. (1999) *p*-Coumaroyltriacetic acid synthase, a new homologue of chalcone synthase, from *Hydrangea macrophylla* var. *thunbergii*. *Eur. J. Biochem.* **263**, 834–839
11. Sankaranarayanan, R., Saxena, P., Marathe, U.B., Gokhale, R.S., Shanmugam, V.M., and Rukmini, R. (2004) A novel tunnel in mycobacterial type III polyketide synthase reveals the structural basis for generating diverse metabolites. *Nat. Struct. Mol. Biol.* **11**, 894–900
12. Austin, M.B., Izumikawa, M., Bowman, M.E., Udwary, D.W., Ferrer, J.L., Moore, B.S., and Noel, J.P. (2004) Crystal structure of a bacterial type III polyketide synthase and enzymatic control of reactive polyketide intermediates. *J. Biol. Chem.* **279**, 45162–45174
13. Funa, N., Ozawa, H., Hirata, A., and Horinouchi, S. (2006) Phenolic lipid synthesis by type III polyketide synthases is essential for cyst formation in *Azotobacter vinelandii*. *Proc. Natl Acad. Sci. USA.* **103**, 6356–6361
14. Funa, N., Awakawa, T., and Horinouchi, S. (2007) Pentaketide resorcylic acid synthesis by type III polyketide synthase from *Neurospora crassa*. *J. Biol. Chem.* **282**, 14476–14481
15. Gross, F., Luniak, N., Perlova, O., Gaitatzis, N., Jenke-Kodama, H., Gerth, K., Gottschalk, D., Dittmann, E., and Muller, R. (2006) Bacterial type III polyketide synthases: phylogenetic analysis and potential for the production of novel secondary metabolites by heterologous expression in pseudomonads. *Arch. Microbiol.* **185**, 28–38
16. Austin, M.B., Saito, T., Bowman, M.E., Haydock, S., Kato, A., Moore, B.S., Kay, R.R., and Noel, J.P. (2006) Biosynthesis of *Dictyostelium discoideum* differentiation-inducing factor by a hybrid type I fatty acid-type III polyketide synthase. *Nat. Chem. Biol.* **2**, 494–502
17. Shomura, Y., Torayama, I., Suh, D.-Y., Xiang, T., Kita, A., Sankawa, U., and Miki., K. (2005) Crystal structure of stilbene synthase from *Arachis hypogaea*. *Proteins* **60**, 803–806
18. Dunham, C.M., Dioum, E.M., Tuckerman, J.R., Gonzalez, G., Scott, W.G., and Gilles-Gonzalez, M.A. (2003) A distal arginine in oxygen-sensing heme-PAS domains is essential to ligand binding, signal transduction, and structure. *Biochemistry* **42**, 7701–7708
19. Edwards, R.A., Whittaker, M.M., Whittaker, J.W., Baker, E.N., and Jameson, G.B. (2001) Outer sphere mutations perturb metal reactivity in manganese superoxide dismutase. *Biochemistry* **40**, 15–27
20. Jez, J.M. and Noel, J.P. (2000) Mechanism of chalcone synthase. pK_a of the catalytic cystein and the role of the conserved histidine in a plant polyketide synthase. *J. Biol. Chem.* **275**, 39640–39646
21. Suh, D.-Y., Kagami, J., Fukuma, K., and Sankawa, U. (2000) Evidence for catalytic cystein–histidine dyad in chalcone synthase. *Biochem. Biophys. Res. Commun.* **275**, 725–730
22. Saslowsky, D.E., Dana, C.D., and Winkel-Shirley, B. (2000) An allelic series for the chalcone synthase locus in *Arabidopsis*. *Gene* **255**, 127–138
23. Ke, S.-H. and Madison, E.L. (1997) Rapid and efficient site-directed mutagenesis by single-tube 'megaprimer' PCR method. *Nucleic Acids Res.* **25**, 3371–3372
24. Suh, D.-Y., Fukuma, K., Kagami, J., Yamazaki, Y., Shibuya, M., Ebizuka, Y., and Sankawa, U. (2000) Identification of amino acid residues important in the cyclization reactions of chalcone and stilbene synthases. *Biochem. J.* **350**, 229–235
25. Yamaguchi, T., Kurosaki, F., Suh, D.-Y., Sankawa, U., Nishioka, M., Akiyama, T., Shibuya, M., and Ebizuka, Y. (1999) Cross-reaction of chalcone synthase and stilbene synthase overexpressed in *Escherichia coli*. *FEBS Lett.* **460**, 457–461
26. Eckermann, S., Schröder, G., Schmidt, J., Strack, D., Edrada, R.A., Helariutta, Y., Elomaa, P., Kotilainen, M., Kilpeläinen, I., Proksch, P., Teeri, T.H., and Schröder, J. (1998) New pathway to polyketides in plants. *Nature* **396**, 387–390
27. Takahashi, K. (1968) The reaction of phenylglyoxal with arginine residues in proteins. *J. Biol. Chem.* **243**, 6171–6179
28. Stöckigt, J. and Zenk, M.H. (1975) Chemical syntheses and properties of hydroxycinnamoyl-coenzyme A derivatives. *Z. Naturforsch.* **30**, 352–358
29. Beuerle, T. and Pichersky, E. (2002) Enzymatic synthesis and purification of aromatic coenzyme A esters. *Anal. Biochem.* **302**, 305–312
30. Thompson, J.D., Gibson, T.J., Plewniak, F., Jeanmougin, F., and Higgins, D.G. (1997) The ClustalX windows interface: flexible strategies for multiple sequence alignment aided by quality analysis tools. *Nucleic Acids Res.* **25**, 4876–4882
31. Schwede, T., Kopp, J., Guex, N., and Peitsch, M.C. (2003) SWISS-MODEL: an automated protein homology-modeling server. *Nucleic Acids Res.* **31**, 3381–3385
32. Guex, N., Diemand, A., and Peitsch, M.C. (1999) Protein modelling for all. *Trends Biol. Sci.* **24**, 364–367
33. Wilmot, C.M. and Thornton, J.M. (1988) Analysis and prediction of the different types of beta-turn in proteins. *J. Mol. Biol.* **203**, 221–232
34. Plapp, B.V. (1995) Site-directed mutagenesis: a tool for studying enzyme catalysis. *Methods Enzymol.* **249**, 91–119
35. Ageez, A., Kazama, Y., Sugiyama, R., and Kawano, S. (2005) Male-fertility genes expressed in male flower buds of *Silene latifolia* include homologs of anther-specific genes. *Genes Genet. Syst.* **80**, 403–413
36. Ferrer, J.-L., Jez, J.M., Bowman, M.E., Dixon, R.A., and Noel, J.P. (1999) Structure of chalcone synthase and the molecular basis of plant polyketide biosynthesis. *Nat. Struct. Biol.* **6**, 775–784
37. Huang, W., Jia, J., Edwards, P., Dehesh, K., Schneider, G., and Lindqvist, Y. (1998) Crystal structure of beta-ketoacyl-acyl carrier protein synthase II from *E. coli* reveals the molecular architecture of condensing enzymes. *EMBO J.* **17**, 1183–1191
38. Qiu, X., Janson, C.A, Konstantinidis, A.K., Nwagwum, S., Silverman, C., Smith, W.W., Khandekar, S., Lonsdale, J., and Abdel-Meguid, S.S. (1999) Crystal structure of β-ketoacyl-acyl carrier protein synthase III. A key

condensing enzyme in bacterial fatty acid biosynthesis. *J. Biol. Chem.* **274**, 36465–36471
39. Tokuriki, N., Stricher, F., Schymkowitz, J., Serrano, L., and Tawfik, D.S. (2007) The stability effects of protein mutations appear to be universally distributed. *J. Mol. Biol.* **369**, 1318–1332
40. Jez, J.M., Ferrer, J.L., Bowman, M.E., Dixon, R.A., and Noel, J.P. (2000) Dissection of malonyl-coenzyme A decarboxylation from polyketide formation in the reaction mechanism of a plant polyketide synthase. *Biochemistry* **39**, 890–902
41. Funa, N., Ohnishi, Y., Ebizuka, Y., and Horinouchi, S. (2002) Alteration of reaction and substrate specificity of a bacterial type III polyketide synthase by site-directed mutagenesis. *Biochem. J.* **367**, 781–789
42. Hemleben, V., Dressel, A., Epping, B., Lukacin, R., Martens, S., and Austin, M. (2004) Characterization and structural features of a chalcone synthase mutation in a white-flowering line of *Matthiola incana* R. Br. (Brassicaceae). *Plant Mol. Biol.* **55**, 455–465
43. Haapalainen, A.M., Merilainen, G., and Wierenga, R.K. (2006) The thiolase superfamily: condensing enzymes with diverse reaction specificities. *Trends Biochem. Sci.* **31**, 64–71
44. Dana, C.D., Bevan, D.R., and Winkel, B.S.J. (2006) Molecular modeling of the effects of mutant alleles on chalcone synthase protein structure. *J. Mol. Model.* **12**, 905–914